Semi-fluorinated phosphonic acids form stable nanoscale clusters in Langmuir–Blodgett and self-assembled monolayers

Siwar Trabelsi,[a] Shishan Zhang,[b] Zhongcheng Zhang,[b] T. Randall Lee[b] and Daniel K. Schwartz*[a]

Received 7th August 2008, Accepted 7th November 2008
First published as an Advance Article on the web 7th January 2009
DOI: 10.1039/b813742k

We compared molecular monolayers of semifluorinated phosphonic acids (**F8H11PO$_3$**, **F10H6PO$_3$**, **F8H8PO$_3$**, and **F6H10PO$_3$**) on mica substrates prepared by two different methods: Langmuir–Blodgett (LB) transfer of pre-formed monolayers from the air–water interface, and self-assembled monolayers (SAMs) formed spontaneously at the interface between mica and solution (with tetrahydrofuran as the solvent). The films were investigated with atomic force microscopy (AFM) and contact angle measurements. Nanometer-scale two-dimensional (2D) clusters (20–30 nm in size) were observed in both the LB films and the SAMs. Time-dependent AFM images suggested that for SAMs derived from **F8H11PO$_3$**, **F8H8PO$_3$**, and **F6H10PO$_3$**, small clusters nucleated, but stopped growing once a stable size was reached. *In situ* AFM images suggested that the clusters were dome-shaped. The LB monolayer structures were consistent with those of the SAMs, but with greater long-range order of the clusters in some cases. For SAMs derived from **F10H6PO$_3$**, however, long immersion times led to continued growth and coalescence of the 2D clusters and formation of a flat, untextured monolayer. Similarly, LB films generated from **F10H6PO$_3$** exhibited cluster coalescence. The similarity of the observed structures in LB films and SAMs suggests that these nanostructured films represent an equilibrium state based on intrinsic self-organization of the semifluorinated molecules, even in SAMs, where mobility is significantly restricted at the solid–liquid interface. Based on these observations, we hypothesize that the packing incommensurability between the hydrocarbon and fluorocarbon blocks leads to splay of neighboring chains and spontaneous curvature. However, when intermolecular interactions are dominated by a long fluorocarbon block, there is a transition to a flat structure, where the packing mismatch is compensated for by increased disorder within the hydrocarbon block.

Introduction

Self-assembled monolayers (SAMs) and Langmuir–Blodgett (LB) films represent the two dominant approaches for preparing monomolecular films on solid substrates. LB deposition involves the initial formation of a monolayer at the air–water interface, followed by the transfer of the monolayer to a solid support by passing that support through the interface.[1,2] Although this approach requires specialized equipment, it provides experimental control of the surface concentration. Also the initial molecular organization at a fluid interface is conventionally believed to result in equilibrated, well-annealed layers. SAMs, on the other hand, form spontaneously at the solid–solution interface by the process of molecular adsorption followed by two-dimensional self-assembly.[3–5] This process is conceptually and experimentally simple and amenable to industrial scale-up. However, since molecular mobility is reduced at the solid–liquid interface, there is widespread concern that the monolayer structure will be kinetically hindered, and will not reach equilibrium on accessible time scales. While both approaches have been extensively studied due to promising applications in areas that include biosensing, lubrication, and corrosion inhibition, direct comparisons of chemically-identical films prepared by the two methods are uncommon.

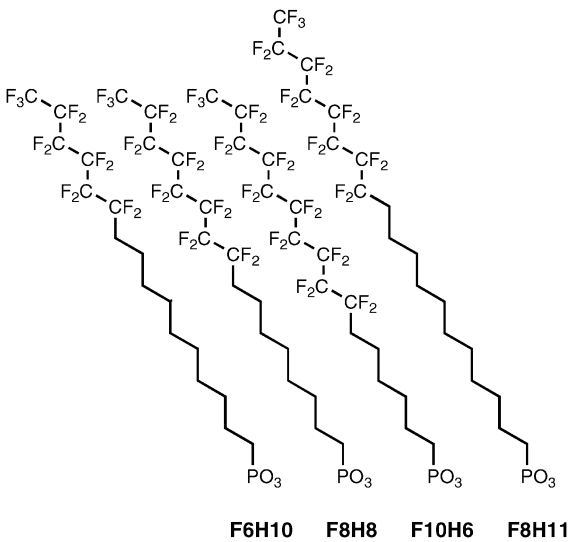

Fig. 1 Structures of phosphonic acids used to prepare films in the present study.

[a]*Department of Chemical and Biological Engineering, University of Colorado, Boulder, CO, 80309-0424, USA. E-mail: Daniel.Schwartz@colorado.edu; Fax: +1 303-492-4341; Tel: +1 303-735-0240*
[b]*Department of Chemistry, University of Houston, Houston, TX, 77204-5003, USA*

In addition to the extensively-studied SAMs derived from alkanethiols[6–8] and alkylsilanes,[9–11] SAMs derived from phosphonic acids such as those shown in Fig. 1 have also inspired increasing interest in recent years for their ability to produce robust and stable monolayers on a variety of oxide substrates.[12–15] Previous atomic force microscope (AFM) studies of hydrocarbon octadecylphosphonic acid (OPA) SAMs on mica substrates suggested a monolayer growth process consisting of the nucleation of compact islands at random locations, growth of these islands, and finally complete coalescence to form homogeneous uniform layers.[16–20] Thus, while clusters were observed during the growth process, they were transient structures, which did not appear at equilibrium.

In previous work, we found that LB monolayers of **F8H11PO$_3$** (Fig. 1), transferred onto mica, exhibited monodisperse clusters[21] with a characteristic size of ~30 nm. Structures with similar length scales have been observed in LB or solution-cast films of other partially-fluorinated compounds as well.[22–24] These structures are intriguing because the associated length scales lie between what would be expected for surface micelles[25,26] (two molecular lengths, or 4–5 nm) and micron-scale domains stabilized by the competition between line tension and electrostatic repulsion.[27–32] The molecular mechanism that gives rise to such clusters is not clear. It has been proposed that the structures result from packing incompatibility of the fluorocarbon and hydrocarbon blocks.[23] However, the structural details sometimes appear to be sensitive to the preparation method;[23] indeed there have been suggestions that similar clusters were the result of kinetic effects[24] and did not represent equilibrium structures at all. Furthermore, with regard to nanoscale structure in LB films, one must always consider the possibility that the structure is caused or modified by the LB transfer process itself.[1,33,34]

These considerations motivated us to investigate SAMs of semi-fluorinated phosphonic acids on mica and to compare the surface morphology observed for both LB films and SAMs. We postulated that if the clusters observed in LB films were intrinsic to monolayers of partially-fluorinated phosphonic acids, they should be insensitive to the formation method, provided that equilibrium can be reached by both methods. Pellerite *et al.*[35] had previously demonstrated the formation of a partially-fluorinated phosphonic acid SAM on alumina using laterally-averaging experimental methods, but they did not characterize the nanoscale film structure. In the experiments reported here, the relative sizes of the hydrogenated and fluorinated blocks were varied systematically to explore the influence of molecular geometry on cluster size and shape (see Fig. 1), and the monolayers were characterized using AFM and contact angle goniometry.

Experimental details

Sample preparation

The synthesis of the semi-fluorinated phosphonic acid **F8H11PO$_3$** was described previously.[21] The other semi-fluorinated molecules were prepared using analogous strategies and methods.

Tetrahydrofuran (THF) (99.9%, Fisher Scientific) was used as a solvent, both for spreading the Langmuir monolayers (LMs) and for immersion of the SAMs. Ultrapure water from a Millipore Milli-Q UV system (resistivity 18.2 MΩ/cm) was used as the subphase for the Langmuir monolayers and for contact angle measurements. The pH of the subphase was adjusted to 3 by adding an aqueous solution of hydrochloric acid (Mallinckrodt). Hexadecane (99%, Fisher Scientific) was also used for contact angle measurements. LMs of semi-fluorinated amphiphiles were prepared by dropwise addition of solution (~1 g/L) at the air–water interface of a commercial Nima Langmuir–Blodgett trough using a gas-tight microliter syringe. After spreading, the monolayers were left for 10 min to ensure evaporation of the solvent. LB films were transferred onto freshly cleaved mica substrates by the upstroke mode of the vertical dipping method at surface pressures of $\Pi = 4$ and $\Pi = 20$ mN/m. SAMs were prepared by immersing freshly cleaved mica into 0.033 g/L, 0.005 g/L or 0.001 g/L solutions held at 50 °C for times ranging from 2 min to 10 h. (Slow precipitation was observed at room temperature.) Samples were found to emerge completely dry from solution, and rinsing with THF caused no measurable change in the film structure or wettability.

AFM characterization

AFM images were acquired with a Nanoscope MMAFM (Digital Instruments, now Veeco) in tapping mode (height contrast). AFM measurements in air used Si tips (Veeco) with a nominal radius of 8 nm and a nominal spring constant of 40 N/m. *In situ* AFM experiments in liquid were performed using silicon nitride tips (Veeco) with a nominal radius of 20 nm and a nominal spring constant of 0.58 N/m. All measurements were made at room temperature (23 ± 1 °C). The *in situ* images of SAMs during formation[16,18–20] were obtained using the Nanoscope tapping mode liquid cell, which consists of a small glass chamber with inlet and outlet ports and a wire clip to hold the cantilever substrate. A Kalrez o-ring (Du Pont) was used to seal the liquid cell against the sample periphery. Before each *in situ* experiment, the liquid cell was washed with soapy water, rinsed thoroughly, and dried with a stream of nitrogen. A 0.005 g/L solution of **F8H8PO$_3$** was introduced into the cell (containing a mica substrate) and AFM images were obtained.

For the *ex situ* AFM images, the size of the 2D clusters was determined using the radial autocorrelation function (RCF) corresponding to each AFM image. This function exhibits maxima at distances corresponding to the average repeat distance of similar objects. Given the close-packed objects observed for complete monolayers, the position of the first maximum corresponds to the average object size. The size and the height of the clusters were also measured by analyzing cross-sectional height profiles from AFM images; for close-packed clusters, the characteristic cluster size was taken as the distance between minima in the cross-section profile. The shape of individual isolated clusters was characterized by the "shoulder width", *i.e.* the distance over which the profile decreased from its maximum to the baseline. An apparent shoulder width is introduced by an imaging artifact involving the convolution of the feature shape and the shape of the AFM tip; *i.e.* even a feature with a perfectly sharp edge will appear to have a gradually decreasing edge profile. Given the tip radius (R) and the feature height (h), this apparent shoulder width (w) is given by $w^2 = 2hR - h^2$. This formula establishes a resolution limit for the sharpness of edges that can be measured.

Contact angle goniometry

Static contact angles were measured using a custom-built contact angle goniometer. A liquid drop of volume 1 μL was formed at the end of a syringe needle and brought into contact with the surface. Once the needle was removed, the contact angle was measured. Values reported are averages of measurements of at least six drops on three independent samples.

Dynamic light scattering

Solutions of **F8H8PO$_3$** (0.25 g/L and 0.033 g/L) dissolved in THF were characterized by dynamic light scattering using a Brookhaven BI-200SM multi-angle laser light scattering system operating with a He-Ne laser (wavelength $\lambda = 633$ nm). The sample temperature was controlled at 25 ± 0.5 °C. The scattered light was detected by a photomultiplier at scattering angle $\theta = 90°$. The output from the photomultiplier was fed into a processor unit, which counted the photons and calculated the normalized intensity autocorrelation function g(t). In all measurements, the autocorrelation function was completely flat, suggesting the absence of **F8H8PO$_3$** aggregates or particles in THF solution.

Results

SAMs derived from different semifluorinated compounds

AFM images of SAMs derived from **F6H10PO$_3$**, **F8H8PO$_3$**, and **F8H11PO$_3$**, and immersed in 0.033 g/L solution for 1 h showed the presence of irregular 2D clusters. Although the clusters had a clear characteristic dimension, no long-range organization was observed (Fig. 2). For solutions of this concentration, longer immersion (for as long as 3 h) did not lead to a measurable structural change, suggesting stable structures. The RCFs of these AFM images showed one broad maximum, which enabled us to measure the cluster sizes in the range 19–23 nm (Table 1), essentially equal given the experimental uncertainties.

For complete SAMs of **F8H11PO$_3$** and **F8H8PO$_3$**, the clusters were closely packed, and no gaps were observed between them, which made it impossible to measure the apparent cluster height. However, as described below, the apparent height of isolated **F8H8PO$_3$** clusters was measured to be 1.0 ± 0.2 nm for quenched samples in air, and 2.1 ± 0.3 nm for clusters measured *in situ* in solution. In the case of **F6H10PO$_3$**, the apparent height of the clusters was found to be only ~0.5 nm, significantly smaller then the extended molecular lengths (≥2 nm). This observation suggests either that the molecules were (1) not fully extended, (2) substantially tilted from the surface normal,[36,37] and/or (3) that the low areas (holes) did not represent bare substrate.[38] These observations are consistent with the infrared spectroscopy results reported by Pellerite and co-workers,[35] who found that the methylene segments of a **F8H11PO$_3$** SAM never reached a fully ordered configuration, even at long immersion times.

SAMs of **F10H6PO$_3$** exhibited qualitatively different behavior than the rest of the series. After immersion for 1 min in 0.033 g/L solution (Fig. 3), large and irregular domains were observed. Careful examination of these domains suggested that they were composed of small clusters with a characteristic size of ~17 nm. After 1 h of immersion, however, the domains completely coalesced, forming a perfectly flat monolayer (Fig. 3). This structural evolution is consistent with what is typically observed for alkylphosphonic acid SAMs on mica, where the nucleation of small clusters is followed by growth and coalescence into a flat and uniform SAM.[15,17–20] It is notable that an increase of the fluorinated part by only two CF_2 groups in the case of **F10H6PO$_3$** induces a qualitative change in the surface morphology and the behavior of the monolayer.

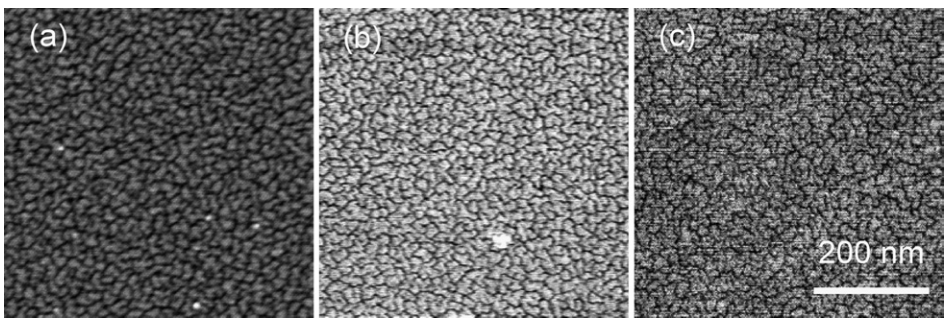

Fig. 2 AFM images of SAMs removed from solution after 1 h immersion in 0.033 g/L solution (in THF) of (a) **F6H10PO$_3$**, (b) **F8H8PO$_3$**, and (c) **F8H11PO$_3$**.

Table 1 Size of the 2D clusters observed on LB films and SAMs (C = 0.033 g/L, t = 30 min for **F8H11PO$_3$**, **F8H8PO$_3$**, and **F6H10PO$_3$** and t = 1 min for **F10H6PO$_3$**)

	LB monolayer cluster size (nm)		SAM cluster size (nm)	
	Autocorrelation function	Cross-section analysis	Autocorrelation function	Cross-section analysis
F6H10PO$_3$	21	19 ± 2	22 ± 1	20 ± 2
F8H8PO$_3$	19 ± 1	19 ± 2	18 ± 1	19 ± 3
F10H6PO$_3$	24 ± 1	21 ± 1	—	17 ± 2
F8H11PO$_3$	30 ± 1	28 ± 2	23 ± 3	21 ± 2

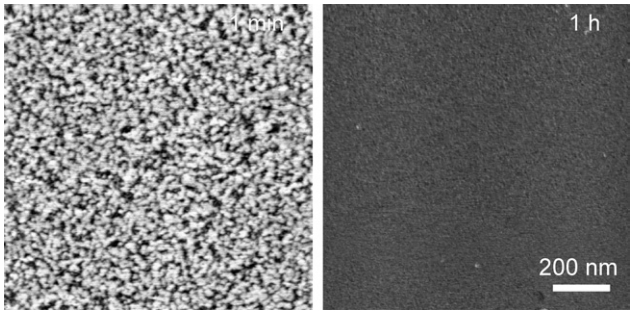

Fig. 3 AFM images of SAMs removed from solution after 1 min and 1 h of immersion in a 0.033 g/L solution of **F10H6PO$_3$**.

Final SAM structure as a function of concentration

The observations reported above indicated that structural differences between SAMs derived from **F6H10PO$_3$**, **F8H8PO$_3$**, and **F8H11PO$_3$** were extremely subtle. Therefore, of these three compounds, we chose one representative example (**F8H8PO$_3$**) for more detailed and systematic kinetic studies. We exposed mica substrates to **F8H8PO$_3$** solutions ranging from 0.001 g/L to 0.033 g/L for increasing immersion times until no further change could be observed with AFM. Representative images of these final structures are presented in Fig. 4. As expected, SAMs prepared from solutions with lower concentrations took longer to reach their final structure. While there may appear to be minor differences between the images in Fig. 4, in fact these differences are no greater than what one might observe on a single sample with different AFM tips. In particular, no quantifiable differences could be observed, and the characteristic cluster sizes are equal within experimental error.

SAM structure as a function of immersion time

Fig. 5 shows representative AFM images of SAMs that were removed from **F8H8PO$_3$** in THF after increasing immersion times.[17] After short immersion times, a few clusters were observed, and the number of clusters increased systematically with immersion time. A narrow but significant range of cluster sizes was observed in the incomplete films; in particular, some very small clusters were visible. However, the maximum cluster size never exceeded the characteristic dimension of clusters in the final film. This observation suggests that while clusters continually nucleated throughout the monolayer formation process, they

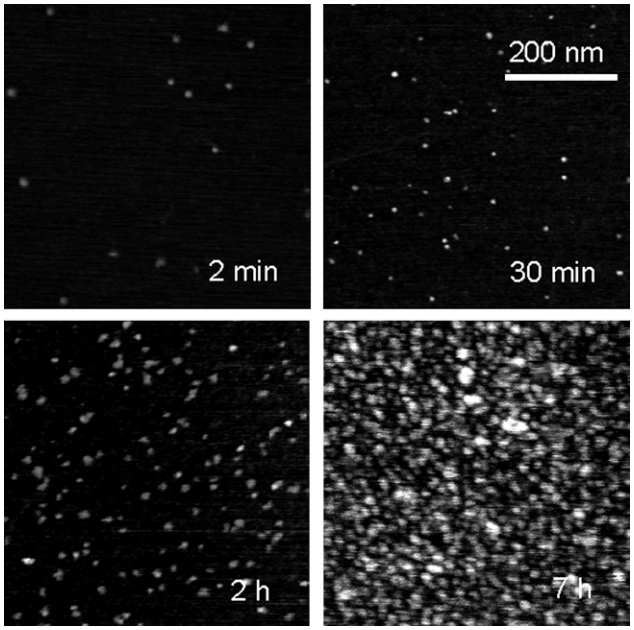

Fig. 5 AFM images of **F8H8PO$_3$** SAMs quenched after various immersion times in 0.002 g/L solution.

did not grow beyond a distinctive maximal dimension. The average apparent height of the isolated clusters was 1.0 ± 0.2 nm. These observations, together with the results from dynamic light scattering measurements, which ruled out the presence of aggregates in solution, suggested that the clusters nucleated on the surface from molecular adsorbates.

In situ AFM characterization of SAMs

Fig. 6 shows a representative *in situ* AFM image of an **F8H8PO$_3$** SAM at the solution–mica interface. In general, the *in situ* images were of lower quality that AFM images of quenched films obtained under ambient conditions, and it was difficult to obtain extended time sequences. However, these images explicitly indicated the presence of molecular clusters consistent with those observed in the quenched SAMs. These *in situ* images represent important control experiments because they prove that the clusters are native structures present during SAM growth, and do not form during removal from solution or drying. Interestingly,

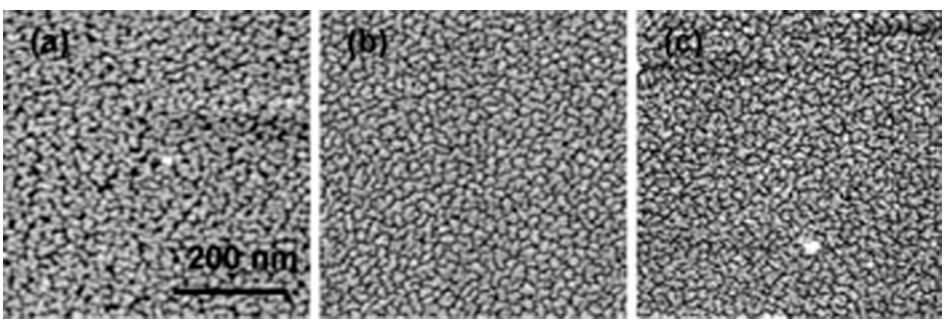

Fig. 4 AFM images of SAMs of pure **F8H8PO$_3$** removed after (a) 10 h of immersion in a 0.001 g/L solution, (b) 7 h of immersion in a 0.005 g/L solution, and (c) 1 h of immersion in a 0.033 g/L solution.

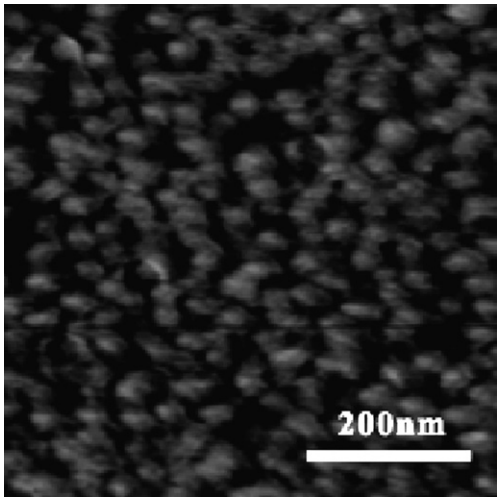

Fig. 6 AFM image obtained *in situ* during monolayer growth on mica in a 0.005 g/L **F8H8PO$_3$** solution after ~2 h of exposure.

the cluster size appeared to be somewhat larger than in the quenched SAMs, suggesting swelling by solvent.

Shape of clusters

When describing the height profile of nanoscale features, one must be cognizant of imaging artifacts due to tip-shape convolution. This phenomenon is particularly complicated given the fact that tip shape varies not only from tip to tip, but also dynamically for an individual tip as it wears and/or accumulates contamination. Thus, we have taken a statistical approach by measuring the shoulder widths for many isolated clusters of **F8H8PO$_3$**. The *in situ* clusters had an apparent height of 2.1 ± 0.3 nm and a shoulder width of 20 ± 3 nm, compared to a resolution limit of ~9 nm based on the nominal tip radius of 20 nm (the maximum tip radius specified by the manufacturer, 40 nm, predicts a resolution limit of 12.5 nm). The clusters measured under ambient conditions had an apparent height of 1.0 ± 0.2 nm and a shoulder width of 10.0 ± 0.2 nm, compared to a resolution limit of ~4 nm (the tips used for tapping mode in air were significantly sharper). Therefore, the measured shoulder width of the clusters was more than twice as large as can be explained by tip-broadening effects, strongly suggesting that the clusters have a gradually sloping or curved shape and do not end abruptly with a sharp edge. Fig. 7 illustrates this analysis with a representative cluster profile. We also note that the cluster shape (lateral size, apparent height, and shoulder width) does depend on the environment; presumably the clusters are swollen in solution.

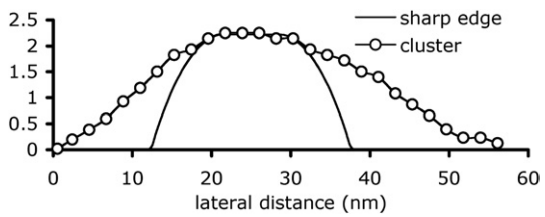

Fig. 7 A representative height profile of an **F8H8PO$_3$** cluster from an *in situ* image compared with a calculated profile for a hypothetical cluster with a perfectly-sharp edge convoluted with a nominal tip shape.

LB monolayers

Representative AFM images corresponding to LB monolayers of **F6H10PO$_3$** and **F8H8PO$_3$** transferred at Π = 4 mN/m are shown in Fig. 8a and 8b, respectively. Both images show the presence of irregular 2D clusters with characteristic sizes of 19–21 nm and with little long-range organization. These clusters are quite stable and resist coalescence even at higher surface pressures (20 mN/m). LB monolayers of **F8H11PO$_3$** transferred at 4 mN/m exhibited organized and extremely monodisperse clusters with a characteristic size of ~30 nm. They have a distinctive shape and a regular, liquid crystalline, arrangement (Fig. 8c) as shown previously.[21] The size of these clusters is slightly larger than those measured for the rest of the series of semi-fluorinated phosphonic acids. Table 1 summarizes the size of the clusters measured using RCF and cross-section analysis for the semi-fluorinated phosphonic acids shown in Fig. 1.

AFM images of **F10H6PO$_3$** LB monolayers transferred at 4 mN/m show monodisperse, organized, and circular 2D molecular clusters (Fig. 9a) along with larger islands of varying size, suggesting the coalescence of clusters. The corresponding radial autocorrelation function (RCF), shown in Fig. 9c, displays well-defined maxima due to the uniformity and organization of the 2D clusters. The average size of the 2D clusters obtained from the RCF is 24 ± 1 nm, slightly larger than the size deduced from an analysis of cross-sections 21 ± 1 nm. In LB monolayers transferred at higher pressure (20 mN/m), the morphology of the AFM image suggests that the clusters coalesce during compression (Fig. 9b).

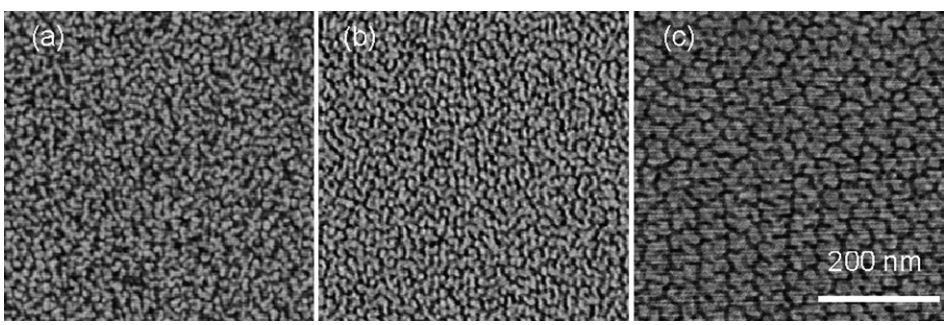

Fig. 8 AFM images of LB films of (a) **F6H10PO$_3$** (b) **F8H8PO$_3$**, and (c) **F8H11PO$_3$**. The monolayers were transferred onto mica at 4 mN/m.

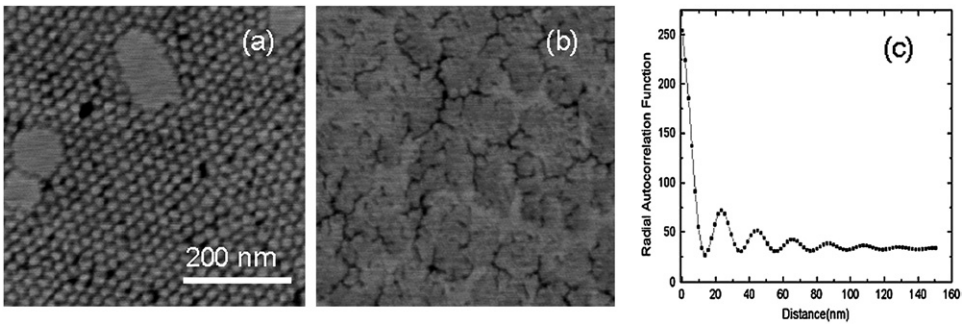

Fig. 9 AFM images **F10H6PO$_3$** LB monolayers transferred onto mica at (a) Π= 4 mN/m and (b) Π= 20 mN/m. (c) Radial autocorrelation function corresponding to Fig. 9a.

Analysis of cross-sections revealed that the height difference between the top of the clusters and the bottom of the holes is ~1 nm for all four materials, significantly smaller than the extended molecular lengths.

Contact angle measurements

The contact angles of hexadecane and water for the LB films and SAMs of **F8H11PO$_3$**, **F10H6PO$_3$**, **F8H8PO$_3$**, and **F6H10PO$_3$** are summarized in Table 2. In general, the contact angles indicate that all of the films are relatively hydrophobic and lipophobic. The high contact angles of hexadecane, in particular, are consistent with expected values for fluorocarbon surfaces.[39] This observation suggests that, in all cases, the fluorocarbon block faces outward as one might expect, and rules out more exotic conformations such as molecular folding or buckling. LB films and SAMs of the phosphonic acid containing the shortest fluorinated segment (**F6H10PO$_3$**) exhibited the smallest contact angle values for both hexadecane and water. Moreover, the contact angles increased as the length of the perfluorinated segment increased. This behavior has been observed for semi-fluorinated thiol-based SAMs on gold,[39] and likely reflects an enhanced packing of the fluorocarbon tailgroups with increasing length of the perfluorocarbon segment.[40] Alternatively, it might be due to the fact that the dipole associated with the CF_2–CH_2 interface becomes more deeply buried with increasing fluorocarbon block length.[41]

Importantly, the contact angles of hexadecane on all of the SAMs were greater for long immersion times compared to shorter immersion times, suggesting a gradual increase in the monolayer coverage, molecular organization, and/or solvent intercalation into the subphase of the monolayer even after the basic nanoscale structure (as probed by AFM) had essentially stabilized. However, the contact angles of water behaved in a similar fashion only for **F10H6PO$_3$**, consistent with the formation of a highly organized monolayer for this molecule as shown in Fig. 3. In contrast, the contact angles of water decreased with immersion time for the SAMs derived from **F8H11PO$_3$**, **F8H8PO$_3$**, and **F6H10PO$_3$**. Furthermore, the contact angles of water decreased by 10–25° when a drop of water was allowed to sit on the surface of the latter SAMs for ~5 min, suggesting that these monolayers are not sufficiently robust to withstand the significant surface stresses imposed at the water three-phase line. Notably, the contact angles of hexadecane were stable for more than 5 min on these SAMs. In contrast, the contact angles of both hexadecane and water were stable for more than 5 min on the LB films.

As a whole, the LB films and the SAMs exhibit contact angles of hexadecane that are roughly identical within experimental error, which is consistent with the similarity of their surface morphologies as imaged by AFM. However, the contact angles of water on the LB films are much larger than those on the SAMs, probably due to the greater stability of the LB films (as indicated above by the absence of dynamic behavior when the LB films were exposed to the contacting probe liquids). We note further that the contact angles of hexadecane on the SAMs of **F8H11PO$_3$** on mica compare favorably with the values previously reported[35] for **F8H11PO$_3$** on alumina.

Discussion

There is a significant literature associated with phase diagrams of monolayers at the air–water interface (Langmuir monolayers, LMs).[5,42,43] In many cases, the nano- and meso-scale

Table 2 Contact angles (in degrees) of hexadecane and water contact for LB films and SAMs (C = 0.033 g/L) on mica. Short immersion times correspond to t = 30 min for **F8H11PO$_3$**, **F8H8PO$_3$**, and **F6H10PO$_3$**, and t = 1 min for **F10H6PO$_3$**. Long immersion times correspond to t = 3 h for **F8H11PO$_3$**, **F8H8PO$_3$** and **F6H10PO$_3$**, and t = 1 h for **F10H6PO$_3$**

	LB monolayers		SAMs – short immersion times		SAMs – long immersion times	
Solvent	Hexadecane	Water	Hexadecane	Water	Hexadecane	Water
F6H10PO$_3$	63 ± 1	62 ± 1	67 ± 1	52 ± 2	76 ± 1	46 ± 1
F8H8PO$_3$	70 ± 1	89 ± 2	73 ± 1	53 ± 1	76 ± 1	51 ± 1
F10H6PO$_3$	73 ± 1	90 ± 1	67 ± 1	68 ± 1	76 ± 1	84 ± 1
F8H11PO$_3$	71 ± 2	91 ± 2	71 ± 1	74 ± 2	77 ± 1	64 ± 1

morphologies (if not the molecular-level details) are preserved upon LB transfer.[1] The ability of LMs to reach thermodynamic equilibrium is intuitively reasonable, given the fluidity of the air–water interface. The question of thermodynamic equilibrium in monolayers and thin films adsorbed on solid surfaces remains more controversial, since the stronger surface adsorption would seem to inhibit mobility. However, there is evidence for some molecular mobility during SAM formation,[18–20,38,44] and also evidence that SAM structure can be sensitive to thermodynamic conditions (*i.e.*, temperature and concentration).[4,14,45–47] In the past, we have observed similar nanoscale structures (cylinders) in LB and self-assembled multilayers of wedge-shaped surfactants.[48,49]

An important result of these experiments is that SAMs of these partially-fluorinated phosphonic acids can indeed be formed on mica substrates, and that these films exhibit nanoscale molecular clusters that are similar in size to those observed in LB monolayers prepared from the same compounds. The characteristic length scales of the SAM nanostructures are independent of solution concentration, suggesting that the molecular clusters are intrinsic features due to molecular self-organization in these molecules, and not a consequence of monolayer growth dynamics. A typical island-growth mechanism of epitaxial growth, for example, would lead to larger islands at lower solution concentration because of a reduced nucleation rate.[20] Furthermore, the appearance of molecular clusters in *in situ* AFM images demonstrates that the clusters are native structures, and not artifacts due to drying, for example.

It is striking that similar nanotextured topography is observed in both SAMs, where molecules gradually accumulate and organize at the THF–mica interface, and LB films, where monolayers are pre-formed at the air–water interface before transfer. This similarity suggests that the characteristic size of the clusters is a consequence of intrinsic packing preferences of the semi-fluorinated molecules when confined to a planar substrate, and that molecules at the solution–solid interface (during SAM growth) are sufficiently mobile to permit the annealing of well-defined structures. The lack of long-range order in the arrangement of clusters in the SAMs, as opposed to that in LB monolayers (of **F10H6PO$_3$** and **F8H11PO$_3$** in particular), suggests that the mobility in SAMs is largely at the molecular level and that large-scale transport does not occur at the solution–solid interface in the same way that it does at the air–water interface.

Since the final cluster size is at least an order of magnitude larger than the molecular dimension, one possibility is that some sort of long-range repulsion may frustrate continuing island growth. This phenomenon is well-known in Langmuir monolayers, where dipole–dipole repulsion gives rise to an increasing energetic cost for large domains. This repulsion is balanced against the line tension, which favors larger domains, leading to a characteristic equilibrium domain size.[27,28,30,32] In Langmuir monolayers, this size is typically much larger than 1 μm.[28] In principle, this mechanism could lead to nanoscale domains; however, it would require extremely small values of line tension.[29] We have shown that these semifluorinated surfactants do serve to lower the line tension in mixed monolayers;[50] however, stabilization of equilibrium domains of this size would require the line tension to be reduced by many orders of magnitude.

The time dependence of the submonolayer topography of **F8H8PO$_3$** is inconsistent with the standard picture of SAM growth (for hydrocarbon SAMs)[4] in which small islands of densely packed molecules nucleate at random locations on the substrate and grow by the adsorption of additional molecules. In the standard model, the islands coalesce, percolate, and finally cover the entire surface. While the 2D clusters formed in the SAMs derived from **F8H11PO$_3$**, **F8H8PO$_3$**, and **F6H10PO$_3$** are observed to nucleate and grow slightly, their size appears to saturate at a fixed characteristic size, and the clusters do not coalesce even for long immersion times. However, SAMs derived from **F10H6PO$_3$** exhibit a growth mechanism that is qualitatively consistent with the standard model, leading to homogenous final layers. Given that the structures of SAMs derived from **F6H10PO$_3$** and **F8H8PO$_3$** are virtually identical, it is interesting that **F10H6PO$_3$**, the next compound in the series, exhibits such dramatically different behavior.

A possible rationalization for the appearance of clusters lies in the incompatibility between the close-packing requirements of the hydrocarbon and fluorocarbon blocks. For example, hexagonal close-packing in an alkanoic acid monolayer (in the rotator phase) corresponds to a nearest neighbor distance of 0.48 nm,[51] while the distance between molecules in the analogous perfluorinated monolayer is 0.585 nm.[52] Semifluorinated molecules can compensate for this incompatibility in several ways while still retaining a flat lamellar structure. For example, tilted chains or disorder (*e.g.*, gauche defects) within the hydrocarbon block can fill extra space to adapt to the preferred fluorocarbon spacing. Another possibility is that continuous, translation-invariant packing will be frustrated, leading to discrete aggregates.

Moeller and coworkers considered a similar system[23] of partially-fluorinated alkanes and proposed two possible simplified models for the unidirectional "ribbons" that they observed; the general principles can be adapted to the current situation. In one extreme case (Moeller's Model I), molecular interactions might be dominated by fluorocarbon–fluorocarbon attraction (this feature is relevant in the limit of long fluorocarbon blocks), in which case the fluorocarbon chains will organize into a well-packed layer, and the hydrocarbon chains are frustrated, but compensate by forming a disordered underlying layer. This situation would lead to a laterally-uniform layer, with a close-packed fluorocarbon stratum atop of a less-organized hydrocarbon layer. In the other scenario (Moeller's Model II), where hydrocarbon–hydrocarbon interactions are significant, and the structure attempts to simultaneously optimize both fluorocarbon and hydrocarbon packing, the slight wedge-shape of the molecule leads to a splayed configuration and spontaneous curvature. The approximate angle associated with such a molecular wedge can be estimated with the formula $\Delta\theta = \Delta d/l$, where Δd refers to the difference between the fluorocarbon and hydrocarbon nearest-neighbor distances and l is the molecular length. This analysis gives a value of $\Delta\theta \approx (0.1\text{ nm})/(2\text{ nm}) = 0.05$. Close-packing of such wedges standing on a flat surface would lead to frustration when the accumulated angle reached π, which would require approximately $\pi/\Delta\theta = 62$ molecules. Given the nearest-neighbor distance of ~0.5 nm, such a cluster would be roughly 30 nm in diameter, similar to what we observe. The dome-like shapes of the **F8H8PO$_3$** clusters observed with AFM are consistent with this picture. This model also suggests that longer molecules would give rise to larger clusters; again consistent with our observations.

We hypothesize that the clusters observed in films prepared from **F6H10PO$_3$**, **F8H8PO$_3$**, and **F8H11PO$_3$** correspond to the sort of aggregate described in Model II, with a splayed molecular configuration. However, the presence of the longer fluorocarbon block in **F10H6PO$_3$** apparently leads to a situation where fluorocarbon–fluorocarbon interactions are more dominant. Although **F10H6PO$_3$** does have some tendency to form the splayed aggregates, as demonstrated by the presence of clusters in LB films at low surface pressures, these aggregates coalesce into a seamless flat layer as the surface coverage increases. This behavior is suggestive of the laterally-homogeneous stratified structure described in Model I, which was predicted for a sufficiently long fluorocarbon block.

Conclusions

AFM images of SAMs derived from **F8H11PO$_3$**, **F8H8PO$_3$**, and **F6H10PO$_3$** on mica exhibit nanoscale clusters with characteristic dimensions of ~20–30 nm that are independent of concentration and do not coalesce even after long immersion times. The images also suggest that the clusters have a curved, dome-like shape. LB monolayers prepared from these compounds also exhibit molecular clusters with similar lateral sizes. The long-term stability of the SAMs and the consistency of length scales between LB films and SAMs suggest that the nanostructured surfaces represent an equilibrium state, even in the case of SAMs where molecular mobility is restricted in comparison with Langmuir monolayers. The submonolayer SAM structure as a function of immersion time suggests that molecular clusters nucleate and begin to grow, but that the growth of a given cluster stops when it reaches a defined size. In contrast, monolayers of **F10H6PO$_3$** form clusters that are prone to coalescence, which eventually leads to the formation of uniform SAMs. Contact angle measurements and AFM images show that the 2D clusters on LB films are more organized and stable than on the SAMs. However, the cluster shape and size were nearly identical in both LB monolayers and SAMs, suggesting that the clusters are a consequence of fundamental packing preferences (*e.g.*, frustration) of the semi-fluorinated amphiphiles. We suggest that, for **F8H11PO$_3$**, **F8H8PO$_3$**, and **F6H10PO$_3$**, packing incompatibility between the fluorocarbon and hydrocarbon blocks leads to a splayed configuration, and the formation of dome-shaped aggregates due to spontaneous curvature. For **F10H6PO$_3$**, on the other hand, the longer fluorocarbon block dominates intermolecular interactions, leading to a stratified laterally-homogeneous structure with an organized upper layer of fluorocarbon atop a sublayer of disorganized hydrocarbon chains.

Acknowledgements

This research was supported by NSF awards DMR-0447585 (ST and DKS) and DMR-0447588 (SZ and TRL). We also thank Ryan Crisman for his assistance with the dynamic light scattering.

References

1 D. K. Schwartz, *Surface Science Reports*, 1997, **27**, 245–334.
2 J. A. Zasadzinski, R. Viswanathan, L. Madsen, J. Garnaes and D. K. Schwartz, *Science*, 1994, **263**, 1726–1733.
3 A. Ulman, *Chemical Reviews*, 1996, **96**, 1533–1554.
4 D. K. Schwartz, *Annual Review of Physical Chemistry*, 2001, **52**, 107–137.
5 C. M. Knobler and D. K. Schwartz, *Current Opinion in Colloid & Interface Science*, 1999, **4**, 46–51.
6 C. D. Bain, E. B. Troughton, Y. T. Tao, J. Evall, G. M. Whitesides and R. G. Nuzzo, *Journal of the American Chemical Society*, 1989, **111**, 321–335.
7 N. Camillone, P. Eisenberger, T. Y. B. Leung, P. Schwartz, G. Scoles, G. E. Poirier and M. J. Tarlov, *Journal of Chemical Physics*, 1994, **101**, 11031–11036.
8 Y. T. Kim and A. J. Bard, *Langmuir*, 1992, **8**, 1096–1102.
9 R. Maoz and J. Sagiv, *Journal of Colloid and Interface Science*, 1984, **100**, 465–496.
10 I. M. Tidswell, B. M. Ocko, P. S. Pershan, S. R. Wasserman, G. M. Whitesides and J. D. Axe, *Physical Review B*, 1990, **41**, 1111–1128.
11 D. K. Schwartz, S. Steinberg, J. Israelachvili and J. A. N. Zasadzinski, *Physical Review Letters*, 1992, **69**, 3354–3357.
12 S. Pawsey, K. Yach and L. Reven, *Langmuir*, 2002, **18**, 5205–5212.
13 P. R. Davies and N. G. Newton, *Applied Surface Science*, 2001, **181**, 296–306.
14 C. Messerschmidt and D. K. Schwartz, *Langmuir*, 2001, **17**, 462–467.
15 J. T. Woodward, A. Ulman and D. K. Schwartz, *Langmuir*, 1996, **12**, 3626–3629.
16 J. T. Woodward and D. K. Schwartz, *Journal of the American Chemical Society*, 1996, **118**, 7861–7862.
17 J. T. Woodward, I. Doudevski, H. D. Sikes and D. K. Schwartz, *Journal of Physical Chemistry B*, 1997, **101**, 7535–7541.
18 I. Doudevski, W. A. Hayes and D. K. Schwartz, *Physical Review Letters*, 1998, **81**, 4927–4930.
19 I. Doudevski and D. K. Schwartz, *Physical Review B*, 1999, **60**, 14–17.
20 I. Doudevski and D. K. Schwartz, *Journal of the American Chemical Society*, 2001, **123**, 6867–6872.
21 S. Trabelsi, S. Zhang, T. R. Lee and D. K. Schwartz, *Soft Matter*, 2007, **3**, 1518–1524.
22 M. Maaloum, P. Muller and M. P. Krafft, *Angewandte Chemie: International Edition*, 2002, **41**, 4331–4334.
23 A. Mourran, B. Tartsch, M. Gallyamov, S. Magonov, D. Lambreva, B. I. Ostrovskii, I. P. Dolbnya, W. H. de Jeu and M. Moeller, *Langmuir*, 2005, **21**, 2308–2316.
24 T. Kato, M. Kameyama, M. Ehara and K. Iimura, *Langmuir*, 1998, **14**, 1786–1798.
25 S. Manne and H. E. Gaub, *Science*, 1995, **270**, 1480–1482.
26 E. J. Wanless and W. A. Ducker, *Journal of Physical Chemistry*, 1996, **100**, 3207–3214.
27 M. Seul and M. J. Sammon, *Physical Review Letters*, 1990, **64**, 1903–1906.
28 H. M. McConnell, *Annual Review of Physical Chemistry*, 1991, **42**, 171–195.
29 D. J. Benvegnu and H. M. McConnell, *Journal of Physical Chemistry*, 1992, **96**, 6820–6824.
30 H. M. McConnell and R. Dekoker, *Journal of Physical Chemistry*, 1992, **96**, 7101–7103.
31 D. J. Benvegnu and H. M. McConnell, *Journal of Physical Chemistry*, 1993, **97**, 6686–6691.
32 H. M. McConnell and R. DeKoker, *Langmuir*, 1996, **12**, 4897–4904.
33 H. D. Sikes, J. T. Woodward and D. K. Schwartz, *Journal of Physical Chemistry*, 1996, **100**, 9093–9097.
34 H. D. Sikes and D. K. Schwartz, *Langmuir*, 1997, **13**, 4704–4709.
35 M. J. Pellerite, T. D. Dunbar, L. D. Boardman and E. J. Wood, *Journal of Physical Chemistry B*, 2003, **107**, 11726–11736.
36 S. Frey, K. Heister, M. Zharnikov, M. Grunze, K. Tamada, R. Colorado, M. Graupe, O. E. Shmakova and T. R. Lee, *Israel Journal of Chemistry*, 2000, **40**, 81–97.
37 J. Genzer, E. Sivaniah, E. J. Kramer, J. G. Wang, M. L. Xiang, K. Char, C. K. Ober, R. A. Bubeck, D. A. Fischer, M. Graupe, R. Colorado, O. E. Shmakova and T. R. Lee, *Macromolecules*, 2000, **33**, 6068–6077.
38 W. A. Hayes and D. K. Schwartz, *Langmuir*, 1998, **14**, 5913–5917.
39 R. Colorado and T. R. Lee, *Langmuir*, 2003, **19**, 3288–3296.

40 H. Fukushima, S. Seki, T. Nishikawa, H. Takiguchi, K. Tamada, K. Abe, R. Colorado, M. Graupe, O. E. Shmakova and T. R. Lee, *Journal of Physical Chemistry B*, 2000, **104**, 7417–7423.
41 E. G. Shafrin and W. A. Zisman, *Journal of Physical Chemistry*, 1962, **66**, 740.
42 V. M. Kaganer, H. Mohwald and P. Dutta, *Reviews of Modern Physics*, 1999, **71**, 779–819.
43 S. Riviere, S. Henon, J. Meunier, D. K. Schwartz, M. W. Tsao and C. M. Knobler, *Journal of Chemical Physics*, 1994, **101**, 10045–10051.
44 A. Honciuc, A. W. Harant and D. K. Schwartz, *Langmuir*, 2008, **24**, 6562–6566.
45 C. Carraro, O. W. Yauw, M. M. Sung and R. Maboudian, *Journal of Physical Chemistry B*, 1998, **102**, 4441–4445.
46 M. Goldmann, J. V. Davidovits and P. Silberzan, *Thin Solid Films*, 1998, **329**, 166–171.
47 J. M. Mellott and D. K. Schwartz, *Journal of the American Chemical Society*, 2004, **126**, 9369–9373.
48 N. Cain, J. Van Bogaert, D. L. Gin, S. R. Hammond and D. K. Schwartz, *Langmuir*, 2007, **23**, 482–487.
49 M. Nelson, N. Cain, C. E. Taylor, B. M. Ocko, D. L. Gin, S. R. Hammond and D. K. Schwartz, *Langmuir*, 2005, **21**, 9799–9802.
50 S. Trabelsi, S. Zhang, T. R. Lee and D. K. Schwartz, *Physical Review Letters*, 2008, **100**, 037802.
51 S. W. Barton, B. N. Thomas, E. B. Flom, S. A. Rice, B. Lin, J. B. Peng, J. B. Ketterson and P. Dutta, *Journal of Chemical Physics*, 1988, **89**, 2257–2270.
52 S. W. Barton, A. Goudot, O. Bouloussa, F. Rondelez, B. H. Lin, F. Novak, A. Acero and S. A. Rice, *Journal of Chemical Physics*, 1992, **96**, 1343–1351.

